CMS Physics Analysis Summary

Contact: cms-pag-conveners-exotica@cern.ch 2010/07/23

Search for Heavy Stable Charged Particles in pp collisions at $\sqrt{s} = 7$ TeV

The CMS Collaboration

Abstract

A signature-based search is performed for heavy stable charged particles (HSCPs) produced in pp collisions at $\sqrt{s} = 7$ TeV, and collected with the CMS detector, using high transverse momentum muon, jet, and missing transverse energy trigger data corresponding to 198 nb^{-1} of integrated luminosity. Momentum and ionization energy loss measurements are used to isolate candidate events with slowly moving, heavy particles. Additionally, tracks passing muon identification requirements are also analyzed for this signature. In both cases, no event passes the selection criteria with an expected background of less than 0.1 events. This result is interpreted within the contexts of (quasi-)stable stau, gluino, scalar top-quark models and cross section limits of about 10^2 pb at 95% C.L. are obtained. Lower limits at 95% C.L. on the mass of stable gluinos are also set at 284 GeV/c^2 with the analysis that uses muon identification and 271 GeV/c^2 when no muon identification is required.

1 Introduction

Heavy Stable (or long-lived) Charged Particles (HSCPs) appear in various extensions to the Standard Model (SM), arising from a new symmetry, a weak coupling, a kinematic constraint, or a potential barrier. A recent review is available in Reference [1], and collider limits include [2–6].

If the lifetime is long compared to the transit time through the detector, then the particle may escape the detector, thereby evading the limits imposed by direct searches for decay products. Nevertheless, a HSCP will be directly observable in the detector through the distinctive signature of a slowly moving, high momentum (p) particle. The low velocity results in an anomalously large ionization-energy loss rate (dE/dx). Since the particle loses energy primarily through low momentum-transfer interactions, even if strongly interacting (R-hadron[1]), it will be highly penetrating and will likely be identified as a muon. The interactions experienced by R-hadrons in matter can lead to charge-flipping, meaning that the particle can change its electric charge to become oppositely charged or neutral. A recent study [7] on the modelling of the nuclear interactions suffered by HSCPs travelling in matter shows that the probability for gluino or sbottom-based R-hadrons to emerge as neutral particles after traversing an amount of material typical of the calorimeters or iron yokes of the LEP, Tevatron or LHC experiments is close to unity. If this prediction turns out to be correct, HSCPs of the kind mentioned above would not be observable in the muon systems of the experiments. Experimental strategies where the requirement of muon-like behaviour for HSCPs is relaxed are therefore mandatory. For this reason the search is performed with two complementary candidate selections, as detailed below.

In this analysis, a signature-based search is performed for HSCPs produced in pp collisions at $\sqrt{s} = 7$ TeV with the CMS detector at the CERN LHC. Data from the initial LHC run from April-July, 2010, at $\sqrt{s} = 7$ TeV, are analyzed. Data were collected with high transverse momentum (p_{T}) muon, jet, and, missing transverse energy ($E_{\mathrm{T}}^{\mathrm{miss}}$) triggers. The analysis isolates HSCP candidates by selecting tracks reconstructed in the inner tracker detector with high dE/dx and high p_{T}. A second selection additionally requires that the tracks be muon identified. For both selections, the candidate's mass is then calculated from the measured p and dE/dx.

2 CMS Detector

A detailed description of the CMS detector can be found elsewhere [8]. The central feature of the CMS apparatus is a 3.8 T superconducting solenoid of 6 m internal diameter surrounding a silicon pixel and strip tracker, a crystal electromagnetic calorimeter (ECAL) and a brass scintillator hadronic calorimeter (HCAL). Muons are measured in gaseous detectors embedded in the iron return yoke. In addition to the barrel and endcap detectors, CMS has extensive forward calorimetry. CMS uses a right-handed coordinate system, with the origin at the nominal collision point, the x-axis pointing to the center of the LHC, the y-axis pointing up (perpendicular to the LHC plane), and the z-axis along the anticlockwise-beam direction. The polar angle, θ, is measured from the positive z-axis and the azimuthal angle, ϕ, is measured in the $x - y$ plane. In the central inner silicon tracker, charged particles are tracked by three layers of silicon pixel detectors, made of 66 million 100×150 μ m^2 pixels, followed by ten microstrip layers, with strips of pitch between 80 and 180 μm. Matching the muons to the tracks measured in the silicon tracker results in p_{T} resolution between 1 and 5%, for p_{T} values up to 1 TeV/c. If, instead,

[1] HSCPs with strong charge will hadronize and form mesons, baryons or gluonballs. These hadronized states are generically called R-hadrons.

only the inner tracker is used, the resolution degrades to 10% at p_{T} values of 1 TeV/c.

Trigger and reconstruction efficiency in the muon detectors is limited by requirements on the arrival time of the tracks to the muon system. These requirements can affect the efficiency for detecting slow HSCPs. The dependence of the muon trigger efficiency on the particle β is studied using Monte Carlo (MC) simulations. The muon trigger efficiency starts dropping linearly at $\beta = 0.7$ and reaches very low values at $\beta = 0.3$.

The dE/dx measurement is currently performed using only the information from the silicon strip detector. The dE/dx measurement is limited by the silicon strip analog-to-digital converter modules (ADC) that are characterized by a maximum number of counts that corresponds to about 3 times the average charge released by a minimum ionizing particle (MIP) in 300 μm of silicon. The latter is the thickness of the modules mounted in the inner barrel silicon strip modules.

3 Trigger and Data Sample

The events used in this analysis are collected with three types of triggers: triggers requiring a single muon ($p_T > 3$ GeV/c) or dimuon pair, triggers requiring $E_{\mathrm{T}}^{\mathrm{miss}} > 45$ GeV (to search for HSCPs emerging mainly neutral after traversing the calorimeters, or just failing muon identification) or triggers requiring one jet ($p_T > 30$ GeV/c) or more to search for HSCPs accompanied by substantial hadronic activity. Data corresponding to an integrated luminosity of 198 nb^{-1} from the initial LHC run from April-July, 2010, at $\sqrt{s} = 7$ TeV, are analyzed.

Two selections are used in this analysis to define HSCP candidates: a "tracker-only" and a "tracker plus muon identification" selection. Both selections require an individual track, reconstructed in the inner tracker detector, that satisfies the standard CMS track reconstruction algorithm [9]. For the muon-like selection, additionally, the track must be loosely identified as a muon (it must be either a "global muon" or "tracker muon", [10]). For both selections, only the associated silicon tracker track is used for the p and dE/dx measurements, and muon candidates sharing the same inner tracker track are vetoed. The particle momentum is taken as the measurement of the track momentum at the point of closest approach to the reconstructed primary vertex.

4 Signal and Standard Model Background

A few simulated signal samples are also used in this analysis. Events with direct production of supersymmetric scalar top squarks ($\tilde{t}_1$) are produced with $\tilde{t}_1$ masses of 130, 200, 300, 500, and 800 GeV/c^2, with the MadGraph generator [11], interfaced to PYTHIA [12] for the showering and hadronization steps; the so called "MLM" [13] matching prescription is applied after showering in order to yield a realistic spectrum of associated gluons. Events with direct pair production of gluino ($\tilde{g}$) of different masses are generated with PYTHIA. Direct pair production of $\tilde{t}_1$ and $\tilde{g}$ is at leading-order model independent as the only relevant parameter is the mass of the $\tilde{t}_1$ and $\tilde{g}$, respectively. The $\tilde{t}_1$ and $\tilde{g}$ are treated as stable in all these samples. Their hadronization is performed by PYTHIA and their interaction with matter is modelled as in Ref. [14]. The fraction of produced R-gluonballs ($\tilde{g}\,g$ state) is an unknown parameter of the hadronization model and affects the fraction of R-hadrons that are neutral at production. In this study, the fraction of produced R-gluonballs is arbitrarily set to 0.1.

Production of supersymmetric quasi-stable leptons ($\tilde{\tau}_1$) at the LHC can proceed either directly or via production of heavier supersymmetric particles (mainly squarks and gluino pairs),

which decay leading to one or more $\tilde{\tau}_1$ particles at the end of the decay chain. The latter process is in general dominant due to the electroweak nature of the direct production process. In this analysis, the minimal gauge mediated supersymmetry breaking (mGMSB) model [15] is selected as a benchmark for lepton-like HSCPs. Two benchmark points on the SPS line 7 [16] are considered. The particle mass spectrum and the decay table are produced with the program ISASUGRA [17] version 7.69. The parameter values corresponding to the two considered points are as follows:

- $\tilde{\tau}(156)$: $N = 3$, $\Lambda = 50000$ GeV, $M = 100000$ GeV, $\tan\beta = 10$, $sign(\mu) = 1$, $c_{grav} = 10000$
- $\tilde{\tau}(247)$: $N = 3$, $\Lambda = 80000$ GeV, $M = 160000$ GeV, $\tan\beta = 10$, $sign(\mu) = 1$, $c_{grav} = 10000$

The corresponding $\tilde{\tau}_1$ masses are 155.8 and 247 GeV/c^2. The squark and gluino masses are of about 1.1 and 1.7 TeV/c^2, respectively. A few more mass points are obtained by varying the Λ parameter in order to cover a mass range from 100 to 300 GeV/c^2. For all points, the squark and gluino production cross sections are between one and two orders of magnitude higher than that of direct $\tilde{\tau}_1$ pair production.

Trigger efficiencies for the signal are as follows: for R-hadrons, the jet and $E_{\mathrm{T}}^{\mathrm{miss}}$ trigger efficiencies range from 25% (low mass) to 85% (high mass), while the muon trigger efficiencies range from 15% (high mass) to 45% (low mass). For the $\tilde{\tau}_1$ signal, the jet and $E_{\mathrm{T}}^{\mathrm{miss}}$ trigger efficiencies are above 60%, while the muon triggers are above 90% efficient. The resulting total trigger efficiency, defined as the logical OR of these triggers, is greater than 50% for R-hadrons and 95% for the $\tilde{\tau}_1$ signal.

A minimum bias MC sample enriched with events at high tranverse momentum-transfer QCD interactions ($\hat{p_T} > 30$ GeV/c) and containing approximately 50 million events is also used in the analysis for comparison with data.

5 Event Selection

Candidates are pre-selected by requiring p_{T} greater than 7.5 GeV/c, a relative uncertainty on the p_T smaller than 0.15 and transverse (longitudinal) impact parameter with respect to the reconstructed primary vertex smaller than 0.25 (2) cm. They must also have at least three hits in the silicon strip tracker detectors, which are used for the dE/dx measurement.

Clean separation between HSCPs and SM particles can be achieved by selecting tracks with high p_{T} and high dE/dx. These two quantities are expected to be uncorrelated for MIPs, while a slow-moving HSCP would have large dE/dx even at high p_{T}.

As an estimator of the degree of compatibility of the observed charge measurements with the MIP hypothesis, a slightly modified version of the so-called Smirnov-Cramer-von Mises [18, 19] estimator[2] is used for the selection based on dE/dx. This estimator (I_{as}) is referred to as a discriminator to distinguish it from a different estimator, defined later, that is used for the HSCP mass reconstruction. The I_{as} discriminator is defined as:

[2]The original Smirnov-Cramer-von Mises estimator does not indicate whether the incompatibility of a sample population with a given hypothesis for the parent probability density function is due to too low or too high tail probabilities. The modification applied to the original form of the estimator addresses precisely this point as this analysis looks at incompatibility with the MIP hypothesis in terms of high ionization and not low one.

$$I_{as} = \frac{3}{N} \times \left(\frac{1}{12N} + \sum_{i=1}^{N} \left[P_i \times \left(P_i - \frac{2i-1}{2N} \right) \right]^2 \right), \quad (1)$$

where N is the number of track hits in the silicon strip detectors, P_i is the probability a MIP would produce a charge equal to or smaller than the observed one for the observed path length, and the summation is over the number of track hits in the silicon strip detectors, ordered in terms of increasing P_i. The I_{as} discriminator takes into account the actual MIP energy loss distributions which are a function of the path length in the sensitive parts of the silicon strip detectors and takes into account the ADC cut-off. The charge probability density functions are obtained using tracks with $p > 5$ GeV/c from events collected with a minimum bias trigger. Non-relativistic HSCP candidates will have I_{as} approaching unity.

Figure 1 shows relatively good agreement between the data and the minimum bias MC sample, as well as strong discriminating power for the HSCP signal using I_{as} and p_{T}. For the case of the MC I_{as} distributions, the effect of having enriched the sample with events with high $\hat{p_T}$ is reflected in the presence of a few high-weight events (low $\hat{p_T}$) in the tails of the distribution. For the muon selection the tails of the I_{as} distribution are populated with comparable contributions by both the low $\hat{p_T}$ sample and the high $\hat{p_T}$ one. The former sample suffers from lack of statistics given that only 2 events are found with $I_{as} > 0.2$. The integral of the MC distribution in the region $I_{as} > 0.15$ is in excellent agreement with the data.

Clusters have been cleaned from anomalous ionization contributions due to overlapping MIP tracks, nuclear interactions and hard δ-rays in the silicon strip tracker detectors. Genuine single tracks produce clusters with most of the physical charge distributed over one or two neighbouring strips and with other strips carrying only the fraction (to a first approximation equal to 10^{-n}, where n is the distance in units of strips) of this charge that is induced via capacitive coupling or cross-talk effects. Clusters with multiple charge maxima, as well as clusters with more than two consecutive strips containing high and comparable charge were rejected. The I_{as} distributions for the tracker-only candidates in the data passing the pre-selection with and without the cluster cleaning procedure are shown in Fig. 2 (left). Figure 2 (right) shows the same distributions for the signal MC sample corresponding to a gluino with mass 200 GeV/c^2, where only reconstructed tracks matched to the simulated HSCP particles are considered. The latter distribution is normalized to the integrated luminosity of the data. Thus, the cluster cleaning procedure rejects background at high ionization without a significant impact on the signal. The background rejection is found to be lower for the muon-like candidates, most likely because muons do not undergo nuclear interactions.

As illustrated by Fig. 3, the I_{as} distribution in data depends on the number of silicon strip clusters used for the dE/dx measurement. Small differences in the distribution are also observed for a fixed number of hits but for different η ranges. The latter differences are due to the different typical path lengths in the different η regions, which result in improved dE/dx resolution, but also to differences in material, which result in different rates of secondary particle production. To increase sensitivity, therefore, candidate HSCPs are divided into subsamples according to the number of silicon strip hits and η interval: $0 < \eta < 0.5$, $0.5 < \eta < 1$, $1 < \eta < 1.5$, $1.5 < \eta < 2$ and $2.0 < \eta < 2.5$. As described in more detail in section 7, optimal thresholds for p_T (I_{as}) are determined by requiring the same background efficiency, obtainable with the p_T (I_{as}) selection alone, in each subsample. The value of the thresholds are, in general, different from subsample to subsample; it is the resulting background efficiency that is common to all subsamples.

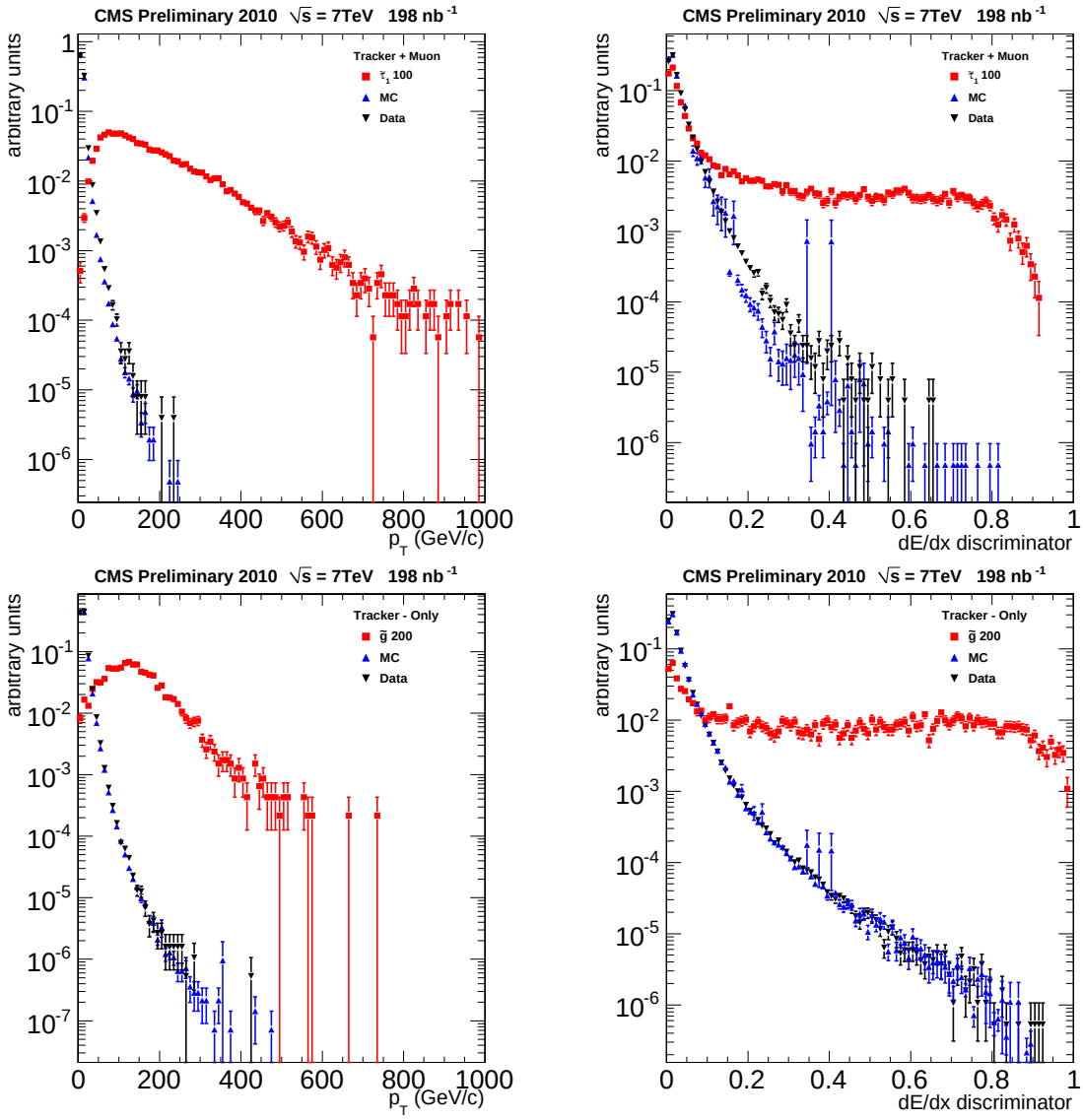

Figure 1: Distributions in data, minimum bias MC, and signal for p_{T} and I_{as}. Upper figures are for the tracker plus muon selection; lower figures are for the tracker only selection. Note that different signal samples are used for the upper and lower figures.

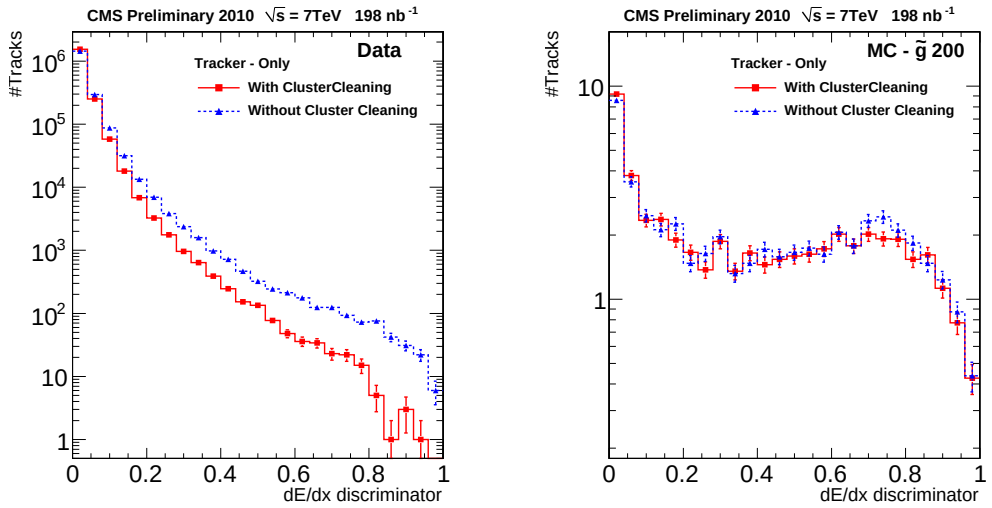

Figure 2: Left: distribution of I_{as} for the tracker-only data candidates passing the pre-selection with and without the cluster cleaning procedure. Right: same distributions for a 200 GeV/c^2 gluino MC sample, where only reconstructed tracks matched to the simulated HSCP particles are considered. This distribution is normalized to the integrated luminosity of the analyzed datasets.

A study performed on MC indicates that a selection that uses the I_{as} discriminator in the place of the I_h estimator increases the signal-to-noise ratio by a factor 3. The division in subsamples according to the track number of hits (η) brings an additional increase by a factor 8 (1.3).

6 Ionization-based Mass Reconstruction

The most probable value of the particle dE/dx is estimated using a harmonic estimator I_h of grade $k = -2$:

$$I_h = \left(\frac{1}{N} \sum_i c_i^k \right)^{1/k} \text{ with } k = -2 \tag{2}$$

where c_i is the charge per unit path length of the i-th hit attached to a given reconstructed track. In order to estimate the mass of highly ionizing particles, the following relationship between I_h, p and m is assumed in the momentum region below that corresponding to the minimum of ionization:

$$I_h = K \frac{m^2}{p^2} + C \tag{3}$$

Equation 3 reproduces with an accuracy of better than 1% the Bethe-Bloch formula in the interval $0.4 < \beta < 0.9$, which corresponds to specific ionizations in the range of 1.1 to 4 times the MIP specific ionization.

Figure 4 (left) shows the distribution of I_h versus p for all reconstructed tracks with at least 12 hits in the silicon strip detector and good primary vertex compatibility from a data sample collected with a minimum bias trigger. The two bands departing towards high I_h values at about 0.7 and 1.5 GeV/c in momentum are due to kaons and protons, respectively, while the

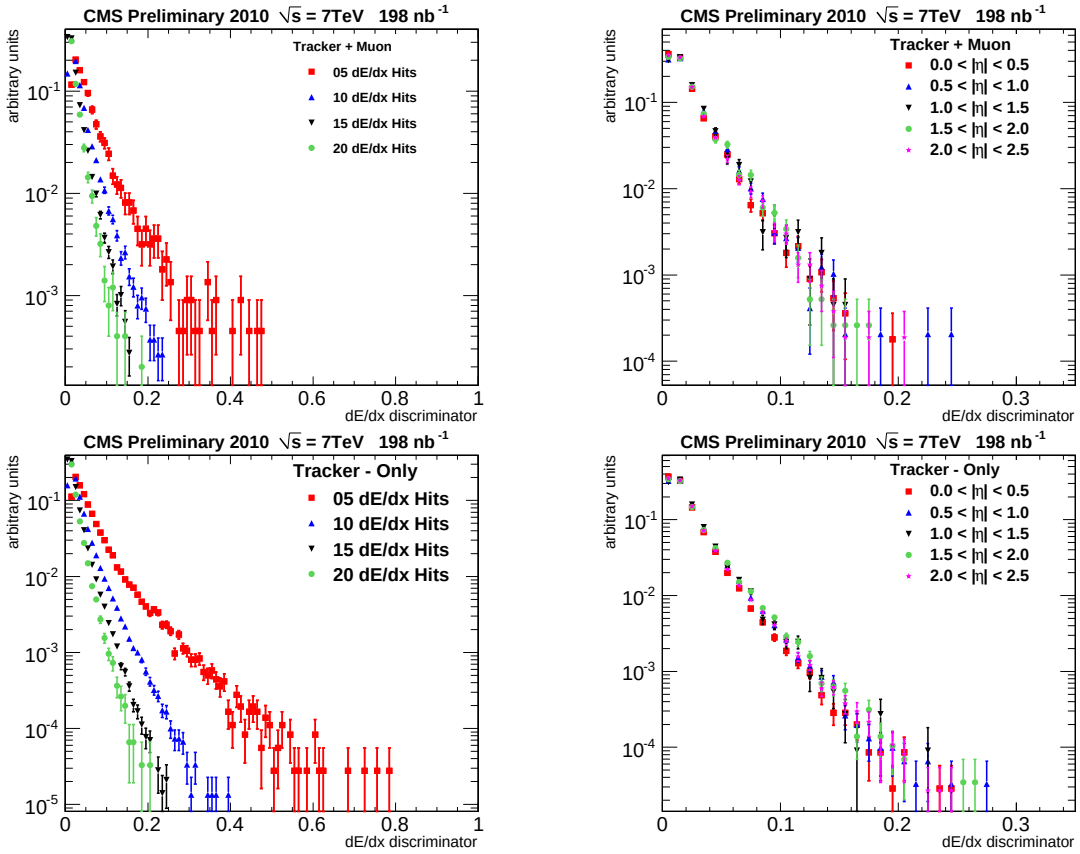

Figure 3: Left: distributions in data of the I_{as} discriminator for tracks with different number of dE/dx measurements. Right: distributions in data of the I_{as} discriminator for tracks with 15 dE/dx measurements and in different η regions. Upper figures are for the tracker plus muon selection; lower figures are for the tracker only selection.

third band is from deuterons. Parameters K and C are determined from a fit to the proton band. The fitted parameters are $K = 2.579 \pm 0.001$ and $C = 2.557 \pm 0.001$.

The mass spectrum obtained using Eq. 3 for all tracks with $I_h > 5$ MeV/cm and $p < 2$ GeV/c is shown in Fig. 4 (right). The known values of the kaon and proton masses are also indicated as vertical lines on the figure. The histogram obtained with MC does not display the deuteron peak because PYTHIA does not produce such particles in pp collisions [9].

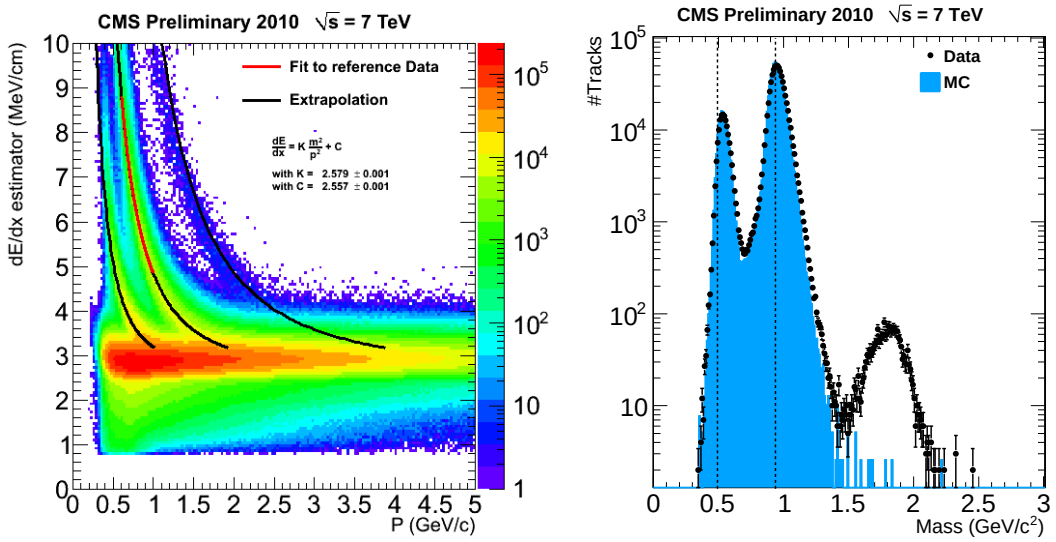

Figure 4: Left: Distribution of the measured p and I_h for all reconstructed tracks with at least 12 hits in the silicon strip detector and good primary vertex compatibility from a data sample collected with a minimum bias trigger. Right: reconstructed mass spectrum in data and MC for all tracks used for the figure on the left, but with $I_h > 5$ MeV/cm and $p < 2.0$ GeV/c. Deuteron production is not simulated in PYTHIA [9].

For mass values of 100 GeV/c^2 or higher, the mass resolution is expected to worsen significantly mainly because of the deterioration of the resolution on the p measurement. Another instrumental effect affecting both the mass scale and the mass resolution is the silicon strip tracker ADC cut-off, which becomes increasingly important as the HSCP β spectrum becomes softer. Indeed, the lower the HSCP β, the higher its dE/dx and, therefore, the higher the chance of having some of its charge measurements truncated. For 300 μm of silicon, truncation starts at β values as low as 0.55. This β threshold grows with the square root of the path length and reaches 1 (MIPs) for path lengths as long as 900 μm. As a consequence, the measured HSCP I_h value will be underestimated and the resulting point in the 2-dimensional p-I_h plane will depart from the corresponding constant-mass curve and populate regions at lower mass values. These effects are visible in Fig. 5, which has been obtained on the MC $\tilde{t}_1$ signal samples. The distribution of I_h and p for all reconstructed tracks passing the pre-selection and matched in direction to the simulated HSCPs in the event are shown in Fig. 5 (left) along with the curves resulting from Eq. 3, where m is set to the nominal $\tilde{t}_1$ mass value. The small cloud of tracks in the lower left corner of the figure is due to mismatched reconstructed tracks produced by non-HSCP particles. Figure 5 (right) shows the resulting mass spectra, normalized to the number of events expected for the integrated luminosity used in this analysis. The degraded mass resolution and the bias in the mass peak position are not relevant for the analysis presented in this document, which is based on a counting experiment, as described in the next section.

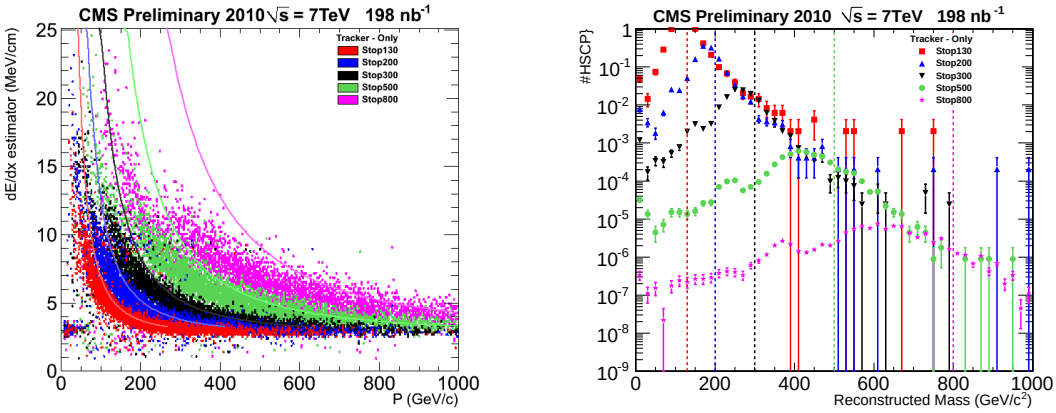

Figure 5: Left: Distribution of the reconstructed p and I_h for all tracks passing the pre-selection and matched to HSCP particles in the $\tilde{t}_1$ MC samples. The curves $I_h = Km^2/p^2 + C$, for the 5 nominal values of the $\tilde{t}_1$ mass, are also drawn. Right: reconstructed mass spectra for these tracks.

7 Background Determination and Search Optimization

The search is performed as a counting experiment in the mass range of 75 to 1200 GeV/c^2 to allow sensitivity to HSCP masses as low as 100 GeV/c^2. For the tracker plus muon identification analysis, which is geared toward the detection of lepton-like HSCPs, the 100 GeV/c^2 $\tilde{\tau}_1$ signal is used for the optimization, while the 200 GeV/c^2 $\tilde{g}$ signal is used to optimize the tracker-only analysis.

The estimation of the background is performed by exploiting the absence of correlation between the p_T and dE/dx measurements. Figure 6 shows the distributions of I_{as} for data for a control sample composed of candidates with $7.5 < p_T < 20$ GeV/c and a signal-like sample composed of candidates with $p_T > 20$ GeV/c. The results obtained for both the tracker-plus-muon and tracker-only candidates are presented. In both cases, the control and signal-like distributions are normalized to unity to allow the shapes to be compared. Good agreement is observed between the two distributions, which indicates that the assumption of lack of correlation between momentum and dE/dx is correct to a good approximation.

A data-driven method that exploits this lack of correlation is therefore employed to estimate the background from MIPs. An estimate of the absolute number of background events passing the selection applied to the ith subsample is obtained as $D_i = B_i C_i / A_i$, where A_i is the number of tracks in the i^{th} subsample that pass neither the I_{as} threshold nor the p_T one chosen for that subsample, B_i (C_i) is the number of tracks that pass only the I_{as} (p_T) threshold, and D_i is the number of tracks that pass both thresholds. By using the mass measurement, this data-driven method is extended to predict the mass spectrum of the background candidates that pass both thresholds. The expected number of retained background events in the search region as predicted by the data-driven technique is computed as a function of the selection, which is defined by the two background efficiency values, common to all subsamples, obtainable with the p_T and the I_{as} selection alone, respectively. These background efficiency values are referred to as ϵ_I and ϵ_{p_T}, respectively. The choice of the selection is, however, also driven by the knowledge of a possible systematic uncertainty on the background estimation. The systematic uncertainty on the expected background in the signal region is estimated by comparing observation and prediction in a control region of the mass spectrum that corresponds to masses smaller than 75 GeV/c^2, following the procedure outlined below. All possible different

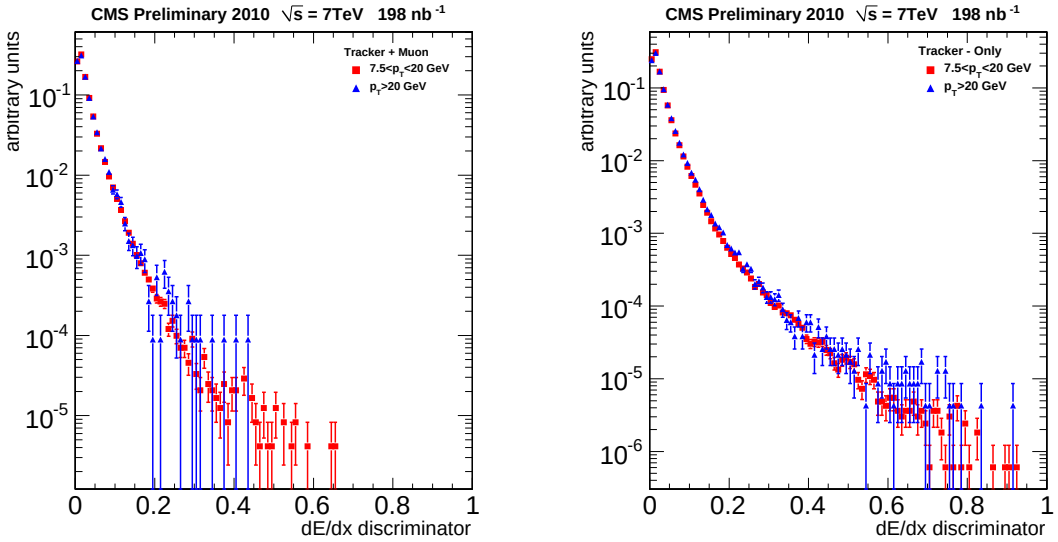

Figure 6: Measured I_{as} distributions for two momentum ranges. Left: tracker plus muon selection, Right: tracker only selection.

selections that provide at least 20 entries in the control region and a total expected background efficiency of at least 10^{-3} are considered, where the total background efficiency is defined as the product of the efficiencies defining the selection. It turns out that for both the tracker-only and the tracker-plus-muon selection the prediction systematically underestimates the observation. The average multiplicative factors that need to be applied to the prediction to match the observation are 1.36 and 1.32 for the tracker-only and tracker-plus-muon selection, respectively. The observed discrepancies could be due to a residual correlation between momentum and dE/dx. For instance, the relativistic rise in the Bethe-Bloch model is not accounted for in the method adopted to estimate the background. Thus, all predictions in the signal region are corrected by the scale factors indicated above. After correcting the prediction for these scale factors, the r.m.s of the distribution of the prediction-to-observation ratio is 0.18 (0.20) for the tracker-only (muon-like) candidates. The relative systematic uncertainty on the corrected background prediction is assumed to be twice these r.m.s. values, the factor of two being a simple safety factor, given that the prediction in the signal region is the relevant quantity for both the choice of the selection and the final results. These uncertainties are much larger than the purely statistical uncertainties for the typical selections adopted in this analysis. In Figure 7 the corrected expected number of background candidates from the data-driven prediction is plotted versus the corresponding number of signal candidates in the search region as predicted by MC. In both analyses, the signal retention does not show a strong dependence on the selection for which 0.01 to 10 background events are expected. An optimal selection is therefore one that retains an expected number of background events of the order of 0.01-0.1. This selection reduces the probability of having one background event in the search region without an excessive reduction of the signal yield. The chosen selections are given in Table 1 and correspond to a remaining background level of about 0.05 events, after correction. A looser selection is also shown.

8 Results

Tables 2 and 3 enumerate the results of this search for the loose and tight selection, respectively. No candidate HSCP tracks are observed in the case of the tight selection for both analyses. In all cases good agreement is found between observations and corrected background predictions.

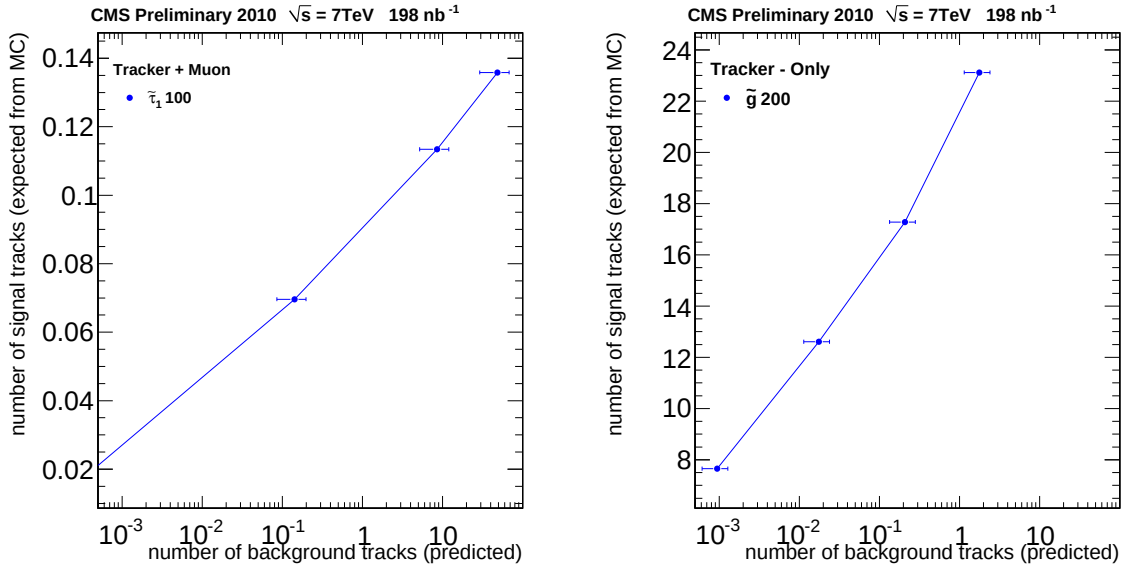

Figure 7: Expected number of signal candidates, as predicted by MC, versus the expected number of background candidates from a data-driven prediction in the search region. Left figure is for the tracker plus muon selection, with the 100 GeV/c^2 $\tilde{\tau}_1$ signal; Right figure is for the tracker only selection, with the 200 GeV/c^2 $\tilde{g}$ signal.

Table 1: Selections used in the analysis. The actual p_{T} and I_{as} thresholds depend on the subsample as explained in the text and are therefore expressed as a range of values. Top: loose selection. Bottom: full (tight) selection.

LOOSE	ϵ_{p_T}	p_T^{cut}	ϵ_I	I_{as}^{cut}
Tracker+Muon	$10^{-1.0}$	7.7 - 25.9	$10^{-1.5}$	0.0036 - 0.4521
Tracker only	$10^{-2.0}$	7.9 - 67.4	$10^{-2.0}$	0.0037 - 0.5293
TIGHT	ϵ_{p_T}	p_T^{cut}	ϵ_I	I_{as}^{cut}
Tracker+Muon	$10^{-3.0}$	7.7 - 125.9	$10^{-3.0}$	0.0036 - 0.6526
Tracker only	$10^{-4.0}$	7.9 - 259.0	$10^{-3.5}$	0.0037- 0.8901

Table 2: Counting experiment results for the loose selection. First two columns: corrected expected and observed number of events in the search region of the mass spectrum. Last two columns: corrected expected and observed number of events in the full mass spectrum.

LOOSE	Exp.	Obs.	Exp. in full spectrum	Obs. in full spectrum
Tracker+Muon	82 ± 33	77	1007 ± 200	838
Tracker Only	108 ± 38	122	184 ± 250	260

Table 3: Counting experiment results for the tight selection. First two columns: corrected expected and observed number of events in the search region of the mass spectrum. Last two columns: corrected expected and observed number of events in the full mass spectrum.

TIGHT	Exp.	Obs.	Exp. in full spectrum	Obs. in full spectrum
Muon-like	0.153 ± 0.061	0	0.249 ± 0.050	0
Tk-only	0.060 ± 0.021	0	0.060 ± 0.011	0

Fig. 8 shows the resulting mass spectra using the loose selection and the corrected predictions. The agreement between MC, corrected data-driven prediction and data in both shape and absolute normalization is satisfactory.

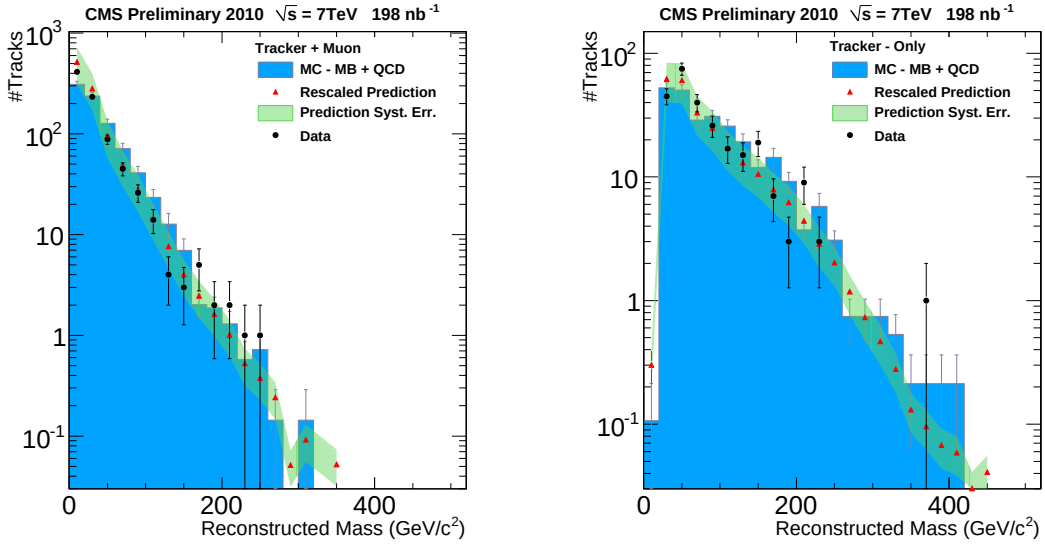

Figure 8: Mass spectra for the loose selection. Left: tracker+muon candidates; right: tracker-only candidates. Observed spectrum (black dots), data-driven corrected predicted background spectrum (full red triangle) with its uncertainty (green band), MC background spectrum (blue histogram).

Fig. 9 shows the distribution of I_h versus p for all the candidates that pass the loose selection. All of the candidates, including one with a measured mass of about 350 GeV/c^2 retained by the tracker-only analysis, are characterized by low I_{as} values that are just above the threshold applied in the corresponding subsample. This is also the case of the few candidates that have I_h values around 5 MeV/cm. These candidates are tracks reconstructed with very few hits, for which the I_{as} threshold is relatively high. Their relatively high I_h values are therefore compatible with background from MIPs.

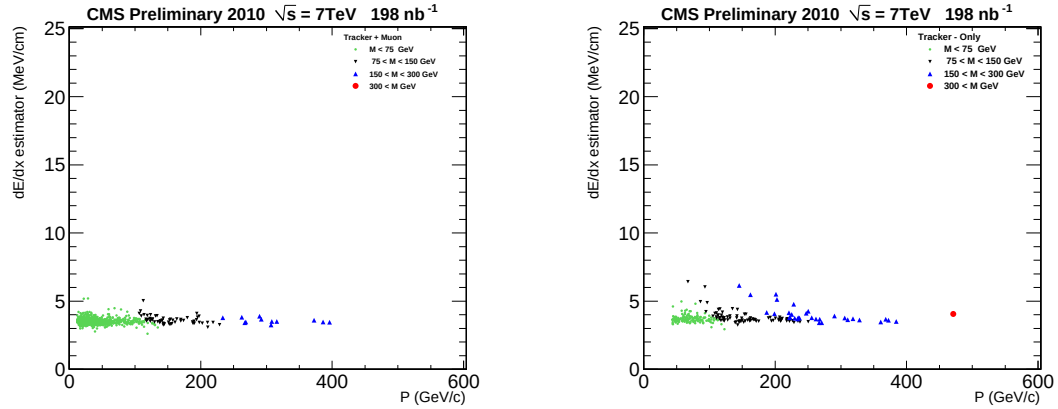

Figure 9: Distribution of the measured p and I_h for all candidates that pass the loose selection. Left: tracker+muon candidates; right: tracker-only candidates.

Given the null result, upper limits are set at 95% C. L. on HSCP production. The acceptance for

gluino mass (GeV/c^2)	200	300	400	500	600	900
Total acceptance (%)	17	21	25	29	29	20
Expected 95% C.L. limit (pb)	106	84	69	60	60	89
Observed 95% C.L. limit (pb)	98	77	64	56	52	83
Theoretical cross section (pb)	606	57.2	8.98	1.87	0.46	0.013
stop mass (GeV/c^2)	130	200	300	500	800	
Total acceptance (%)	12	19	24	30	25	
Expected 95% C.L. limit (pb)	139	91	74	58	72	
Observed 95% C.L. limit (pb)	128	85	68	53	67	
Theoretical cross section (pb)	109	11.9	1.23	0.047	0.00123	
stau mass (GeV/c^2)	100	126	156	200	247	308
Total acceptance (%)	23	34	44	55	63	67
Expected 95% C.L. limit (pb)	76	53	40	32	28	27
Observed 95% C.L. limit (pb)	70	49	37	30	26	25
Theoretical cross section (pb)	1.32	0.33	0.105	0.025	0.008	0.002

Table 4: Acceptances and cross section upper limit for the different models considered with the tracker+muon analysis.

the signal is determined from MC and is given for the two analyses in Table 4 and Table 5. The cross section upper limits at 95% C.L. are computed with a full Bayesian method that uses a lognormal prior [18, 19] for integration over the nuisance parameters. In order to obtain a more conservative upper limit the assumption of no expected background event is used. Resulting cross-section limit curves are provided in Figure 10, along with theoretical expectations for the production of staus, stops, and gluinos. The systematic uncertainties discussed in section 9 are already included in the cross-section upper limits reported in Tables 4 and 5 and Fig 10. The stop (gluino) cross section is computed at NLO (NLO+NLL) [20–22] using PROSPINO [23]. As discussed in section 9, a relative uncertainty of 15% is assumed for these cross sections. From the intersection of the cross-section limit curve obtained with the tracker-plus-muon identification (tracker-only) analysis and the lower edge of the gluino theoretical cross-section band, a 284 (271) GeV/c^2 lower limit at 95% C.L. on the mass of pair produced stable gluinos, hadronizing into R-gluonballs in 10% of the cases, can be set.

9 Systematic Uncertainties

The main sources of systematic uncertainties on the cross section upper limit and mass lower limit results are the following:

- Uncertainty on the signal acceptance. A value of 20% is assumed. It derives from the following contributions:
  - Uncertainty on the trigger efficiency obtained from MC. The uncertainty on the jet and E_t^{miss} trigger efficiency is expected to be dominated by the uncertainty of 10% on the jet energy scale [24]. Varying by $\pm$10% the threshold on the single jet (E_t^{miss}) trigger resulted in a change in the corresponding trigger efficiency by $<$ 5% (max 10%) for all considered signals. A disagreement of up to 10% is observed between the single muon trigger efficiency in data and MC at all energies [10]. In addition, for this specific analysis, it is expected that a further uncertainty may arise as a result of the delayed arrival of HSCPs in the muon system. Assuming a drop in the

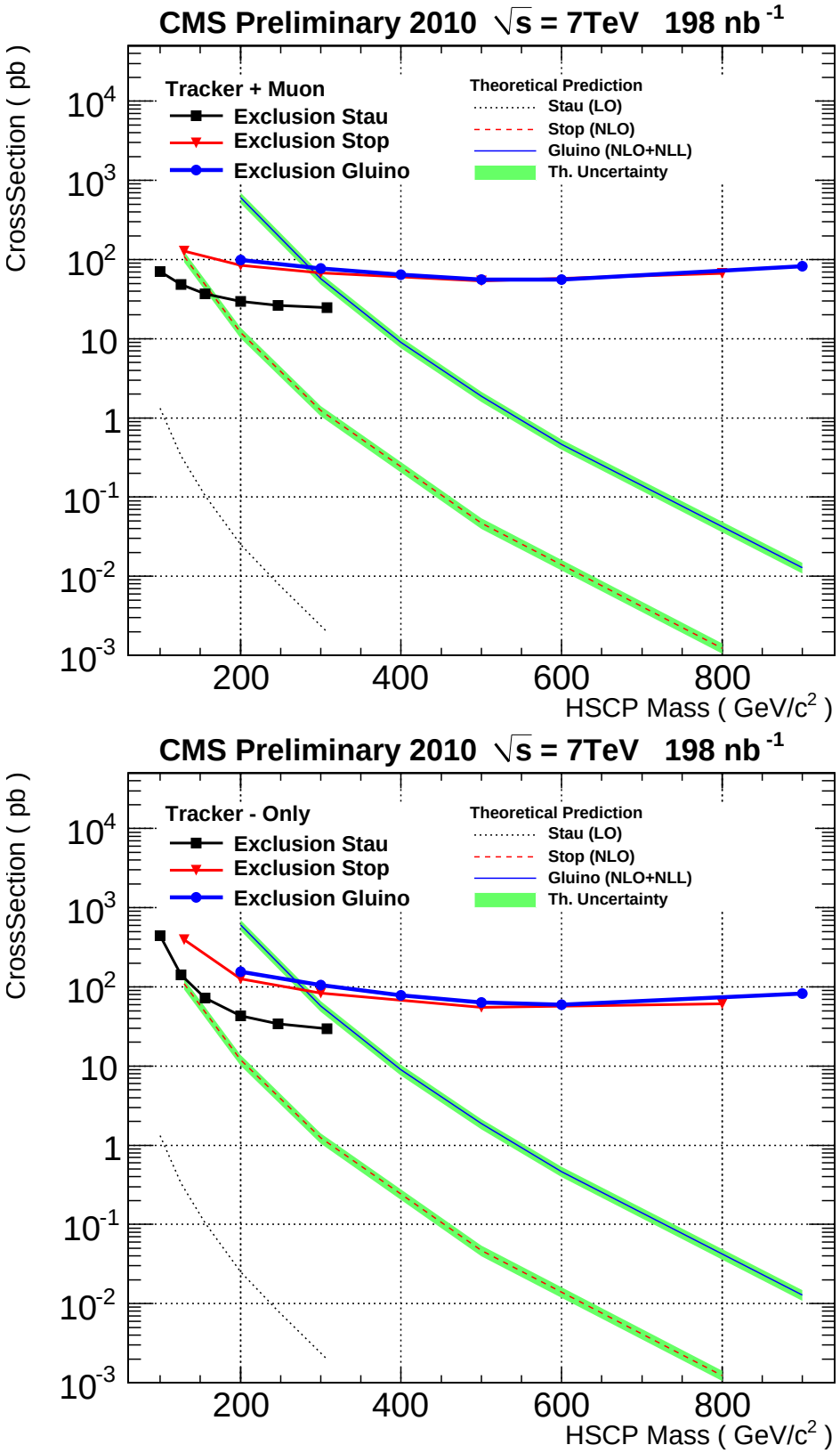

Figure 10: Observed 95% C.L. upper limits on the cross section for production of the different models considered and predicted theoretical cross sections. Upper: analysis of the muon identification plus tracker candidates; Lower: analysis of the tracker-only candidates. The bands represents the theoretical uncertainty on the cross section values.

gluino mass (GeV/c^2)	200	300	400	500	600	900
Total acceptance (%)	11	16	21	26	28	20
Expected 95% C.L. limit (pb)	161	109	81	66	61	85
Observed 95% C.L. limit (pb)	156	105	78	63	59	83
Theoretical cross section (pb)	606	57.2	8.98	1.87	0.46	0.013
stop mass (GeV/c^2)	130	200	300	500	800	
Total acceptance (%)	4	13	20	29	27	
Expected 95% C.L. limit (pb)	409	131	87	57	63	
Observed 95% C.L. limit (pb)	395	127	84	55	61	
Theoretical cross section (pb)	109	11.9	1.23	0.047	0.00123	
stau mass (GeV/c^2)	100	126	156	200	247	308
Total acceptance (%)	4	12	23	38	48	56
Expected 95% C.L. limit (pb)	461	146	74	45	35	31
Observed 95% C.L. limit (pb)	445	141	72	43	34	29
Theoretical cross section (pb)	1.32	0.33	0.105	0.025	0.008	0.002

Table 5: Acceptances and cross section upper limit for the different models considered with the tracker only analysis.

muon trigger efficiency by 15%, it was verified that the drop in the overall trigger efficiency is less than 5% for all considered signals. On the basis of these numbers, an uncertainty of 15% on the overall trigger efficiency was assumed.

- Uncertainty on offline track ($<$ 5% [25]) and muon (5% [10]) reconstruction efficiency.
- Uncertainty on the track momentum scale ($<$ 5% [25]) and dE/dx scale. The latter is estimated to be less than 5% from the level of agreement observed between data and MC for low momentum hadrons ([9] and Fig. 4). It was verified that even a change by 5% in the momentum scale implies a less than 5% change in the signal acceptance. For the case of dE/dx the resulting variation, for the same relative change, is less than 3% for $\tilde{t}_1$ and $\tilde{g}$ and increases to 8% at 100 GeV/c^2 in the case of the $\tilde{\tau}_1$.
- Uncertainty on the models of hadronization and nuclear interactions experienced by R-hadrons. These uncertainties are extremely difficult to estimate and for this reason, it is chosen to treat these models as part of the physics models considered.

- Uncertainty on the absolute value of the integrated luminosity. An uncertainty of 11% is assumed [26].
- Uncertainty on the expected background. This contribution was discussed in Section 7 and is estimated to be 36% (40%) for the tracker-only (tracker plus muon identification) analysis. This uncertainty has, however, a very minor impact on the cross section upper limits for the case at hand of no observed events. In addition, as specified in section 8, the estimate of zero expected background events was used in order to obtain conservative upper limits.
- Uncertainty on the theoretical cross section for production of top squarks and gluino pairs. An uncertainty of 10% arising from the renormalization and factorization scales is assumed on the basis of the study in [20–22], where these uncertainties are quoted to be less than 10% in pp collisions at 14 TeV. These uncertainties are not

Source of Systematic Error	Relative Uncertainty (%)
Theoretical cross section	15 ($\tilde{t}_1$and $\tilde{g}$)
Expected background	36(Tk) ; 40 (Tk+Mu)
Integrated luminosity	11
Trigger efficiency	15
Muon reconstruction efficiency	5
Track reconstruction efficiency	< 5
Momentum scale	< 5
Ionization energy loss scale	< 3 (8 for 100 GeV/c^2 $\tilde{\tau}_1$)
Total uncertainty on signal acceptance	20

Table 6: Sources of systematic errors and corresponding relative uncertainties.

expected to vary significantly with the energy. The relative uncertainty arising from the parton distribution functions is assumed to be 10%, leading to an estimated total relative uncertainty of 15% on the theoretical cross section values. The uncertainty on the theoretical cross section for production of staus in the considered models has not been estimated at this stage.

These uncertainties are summarized in Table 6 and are already incorporated in the quoted limits.

10 Conclusion

In conclusion, the CMS inner tracker has been used to identify highly ionizing, high-p_T tracks as well as measure their masses. A first search is based on all tracks reconstructed in the inner tracker detector. The search was repeated by restricting the selection to highly penetrating tracks identified with the CMS muon system. For both selections, the observed mass distribution is consistent with the expected background from MIPs. From this result, obtained with 198 nb^{-1} of integrated luminosity, an upper limit at 95% C. L. on the production cross section of pairs of stable gluinos, hadronizing into R-gluonballs in 10% of the cases, and top squarks is set at around 100 pb starting from a mass of 130 and 200 GeV/c^2, respectively. For the case of gluinos a mass lower limit of 284 GeV/c^2 can be set at 95% C. L. with the analysis that uses muon identification. This limit becomes 271 GeV/c^2 when no muon identification is required. Cross section upper limits are also set for some benchmark points in the framework of the mGMSB model, predicting the existence of stable staus.

References

[1] M. Fairbairn et al., "Stable massive particles at colliders", *Phys. Rept.* **438** (2007) 1–63, arXiv:hep-ph/0611040. doi:10.1016/j.physrep.2006.10.002.

[2] F. Abe et al., "Search for heavy stable particles in 1.8-TeV $p\bar{p}$ collisions at the Fermilab collider", *Phys. Rev. Lett.* **63** (Oct, 1989) 1447–1450. doi:10.1103/PhysRevLett.63.1447.

[3] F. Abe et al., "Limits on the production of massive stable charged particles", *Phys. Rev. D* **46** (Sep, 1992) R1889–R1894. doi:10.1103/PhysRevD.46.R1889.

[4] D. Acosta et al., "Search for Long-Lived Charged Massive Particles in $p\bar{p}$ Collisions at $\sqrt{s} = 1.8$ TeV", *Phys. Rev. Lett.* **90** (Mar, 2003) 131801. doi:10.1103/PhysRevLett.90.131801.

[5] V. M. Abazov et al., "Search for Long-Lived Charged Massive Particles with the D0 Detector", *Phys. Rev. Lett.* **102** (Apr, 2009) 161802. doi:10.1103/PhysRevLett.102.161802.

[6] T. Aaltonen et al., "Search for Long-Lived Massive Charged Particles in 1.96 TeV $p\bar{p}$ Collisions", *Phys. Rev. Lett.* **103** (Jul, 2009) 021802. doi:10.1103/PhysRevLett.103.021802.

[7] R. Mackeprang and D. Milstead, "An Updated Description of Heavy-Hadron Interactions", *Eur. Phys. J.* **C66** (2010) 493–501, arXiv:0908.1868. doi:10.1140/epjc/s10052-010-1262-1.

[8] CMS Collaboration, "The CMS experiment at the CERN LHC", *JINST* **0803** (2008) S08004. doi:10.1088/1748-0221/3/08/S08004.

[9] CMS Collaboration, "Tracking and Vertexing Results from First Collisions", *CMS Physics Analysis Summary, TRK-10-001* (2010).

[10] CMS Collaboration, "Performance of CMS muon reconstruction in pp collisions at $\sqrt{s} = 7$ TeV", *CMS Physics Analysis Summary, MU-10-002* (2010).

[11] F. Maltoni and T. Stelzer, "MadEvent: automatic event generation with MadGraph", *Journal of High Energy Physics* **2003** (2003), no. 02, 027.

[12] T. Sjostrand, S. Mrenna, and P. Z. Skands, "PYTHIA 6.4 Physics and Manual", *JHEP* **05** (2006) 026, arXiv:hep-ph/0603175.

[13] J. Alwall, S. de Visscher, and F. Maltoni, "QCD radiation in the production of heavy colored particles at the LHC", *JHEP* **02** (2009) 017, arXiv:0810.5350. doi:10.1088/1126-6708/2009/02/017.

[14] R. Mackeprang and A. Rizzi, "Interactions of coloured heavy stable particles in matter", *Eur. Phys. J.* **C50** (2007) 353–362, arXiv:hep-ph/0612161. doi:10.1140/epjc/s10052-007-0252-4.

[15] G. F. Giudice and R. Rattazzi, "Theories with gauge-mediated supersymmetry breaking", *Phys. Rept.* **322** (1999) 419–499, arXiv:hep-ph/9801271. doi:10.1016/S0370-1573(99)00042-3.

[16] B. C. Allanach et al., "The Snowmass points and slopes: Benchmarks for SUSY searches", *Eur. Phys. J.* **C25** (2002) 113–123, arXiv:hep-ph/0202233. doi:10.1007/s10052-002-0949-3.

[17] F. E. Paige, S. D. Protopopescu, H. Baer et al., "ISAJET 7.69: A Monte Carlo event generator for p p, anti-p p, and e+ e- reactions", arXiv:hep-ph/0312045.

[18] W. T. Eadie, D. Drijard, F. E. James et al., "Statistical Methods in Experimental Physics". North Holland, Amsterdam, 1971.

[19] F. James, "Statistical Methods in Experimental Physics, 2nd Edition". World Scientific, Singapore, 2006.

[20] A. Kulesza and L. Motyka, "Threshold Resummation for Squark-Antisquark and Gluino-Pair Production at the LHC", *Phys. Rev. Lett.* **102** (Mar, 2009) 111802. doi:10.1103/PhysRevLett.102.111802.

[21] A. Kulesza and L. Motyka, "Soft gluon resummation for the production of gluino-gluino and squark-antisquark pairs at the LHC", *Phys. Rev. D* **80** (Nov, 2009) 095004. doi:10.1103/PhysRevD.80.095004.

[22] W. Beenakker et al., "Soft-gluon resummation for squark and gluino hadroproduction", *JHEP* **12** (2009) 041, arXiv:0909.4418. doi:10.1088/1126-6708/2009/12/041.

[23] W. Beenakker, R. Hopker, and M. Spira, "PROSPINO: A program for the PROduction of Supersymmetric Particles In Next-to-leading Order QCD", arXiv:hep-ph/9611232.

[24] CMS Collaboration, "Jet performance in pp Collisions at $\sqrt{s} = 7$ TeV", *CMS Physics Analysis Summary, JME-10-003* (2010).

[25] CMS Collaboration, "Measurement of Tracking Efficiency in CMS", *CMS Physics Analysis Summary, TRK-10-002* (2010).

[26] CMS Collaboration, "Measurement of CMS Luminosity", *CMS Physics Analysis Summary, EWK-10-004* (2010).